Time-dependent description of dephasing processes in adsorbate bonding by pumped sum-frequency generation spectroscopy

A. A. Villaeys and F. P. Lohner
Institut de Physique et Chimie des Matériaux de Strasbourg 23, rue du Loess, 67037 Strasbourg Cedex, France
(Received 15 September 1999; revised manuscript received 11 July 2000; published 12 December 2000)

Previous studies on five-wave mixing processes based on Gaussian pulses were restricted to dephasing times shorter than any light pulse duration of the pump and probe beams. Therefore, they do not allow an analysis of the dephasing processes taking place on the bonding mode of the molecular adsorbates. Here we give a description of time-resolved profiles obtained from pumped sum-frequency generation spectroscopy which is valid over the full range of the dephasing times. This enables a detailed analysis of the dephasing processes acting on the adsorbate bonding mode. In particular, we show that pure dephasing processes acting on different vibrational transitions can be analyzed by adopting different resonant conditions for the infrared probe beam. Also, the high sensitivity of the sum-frequency generation signal intensity to the dephasing constants and to the relative values of the field amplitudes is stressed. The model correctly reproduces the experimental data obtained on the C-H stretching modes of hydrogen-terminated F/C(111)-(1×1).

DOI: 10.1103/PhysRevA.63.013810 PACS number(s): 42.65.Ky

I. INTRODUCTION

Sum-frequency generation was used extensively to develop a vibrational spectroscopy on noncentrosymmetric media, like molecular adsorbate or surface and interface states of metals and semiconductors [1–6]. Former measurements of the vibrational relaxation lifetimes, obtained from spectral analysis [7], were misleading because of the dominating contribution to the infrared linewidth of an adsorbate vibration provided by pure dephasing processes [8]. To circumvent this difficulty, vibrational relaxation lifetimes were determined by using the transient bleaching method in conjunction with sum-frequency generation (SFG) spectroscopy [9]. While measurements of population and relaxation rates were first performed in semiconductor surfaces by free-induction decay and photon-echo experiments to probe the coherence of H adsorbed on Si(111) [10], the first measurement of a vibrational coherent transient of CO adsorbed on a metal surface of Cu(111) was realized as soon as higher time resolution, needed for the metal surfaces, became accessible [11]. In addition, it was mentioned that SFG spectra display interferences which are induced by the cross terms between the resonant and nonresonant contributions of the second-order susceptibility [12–14]. These interferences enable a determination of the relative amplitude and phase of the resonant and nonresonant parts. From the spectral analysis of these interferences, the band center and the linewidth of the vibrational resonance of the surface SFG spectrum of CO on Cu(111) are consistent with the results obtained in reflection-absorption infrared spectroscopy experiments [15]. Moreover, infrared-visible SFG was used by Chin *et al.* [16] to obtain the vibrational spectrum of hydrogen on diamond C(111). From a fully relaxed 1×1 surface, they were able to observe a single sharp peak at approximately 2830 cm^{-1}, which can be identified as the CH stretching mode from H on top sites, and that with the surface freshly transformed from 2×1 to 1×1 structure. However, another peak at a higher frequency was detected, which is attributed to H adsorbed on a metastable 1×1 structure.

In fact, a complete understanding of the nonlinear response of molecular adsorbates requires a microscopic description. This is quite difficult since it involves not only an accurate description of the electronic and vibrational structures of the adsorbate and substrate, but also a description of the dynamical processes taking place between the adsorbate and substrate. Concerning the electronic part, but for relatively simple systems, complications arise due to the fact that the excited adsorbate and substrate states, participating in the dynamical response, come into play. Systems like Na on Al(111) were studied [17], and emphasized the complexity of the problem. Moreover, using band-structure calculations and a pseudopotential for the adsorbed alkali-metal atom, it was demonstrated that a strong enhancement of SFG at metal surfaces by adsorbates can be obtained [18]. In addition, the microscopic processes underlying this enhancement were discussed on the basis of a quantum theory. Typical behaviors for acceptors and donors were analyzed. In fact, donors induce a decrease of the SFG signal subsequent to the chemisorption-induced charge transfer in connection with the second-order response of the image with respect to the plane of the substrate, showing a weak dependence on the pump frequency and the nature of the adatom. In the case of acceptors, or covalently bonded atoms, an increase is observed, arising from the nonlinear polarizability of the adatom itself [19].

In addition to studies dedicated to the role of the electronic structure in the nonlinear response of the adsorbate and substrate, many works were devolved to a study of their vibrational structure. In fact, it is now well established that the vibrational line shape of an atom or molecule adsorbed on a surface can be affected by several types of dynamical processes including mainly emission of electron-hole pairs [20–22], emission and absorption of phonons [23,24], and dephasing via phonons and other vibrational modes [23,25–27], as well as dephasing via electron-hole pairs [28]. A number of theoretical studies, based on simplified models [22,23,29–32], was dedicated to a description of the infrared-absorption line shape of an internal vibrational

mode of an adsorbed molecule. In addition to the role of the surface heterogeneity, this line shape is, of course, influenced by all the relaxation and pure dephasing processes taking place because of the interactions existing between the adsorbate vibrational mode and localized or delocalized phonon modes, even with low-lying electronic excitations at a metal surface [20,33]. All these interactions induce a shift and a broadening of the homogeneous vibrational line shape. Models based on lower-order perturbation were developed to evaluate the vibrational relaxation of single diatomic molecules like CO adsorbed upright on metal surfaces [22,31,32]. The homogeneous linewidth of their internal stretching modes results mainly from pure dephasing processes induced by anharmonic coupling with other low-frequency localized or delocalized vibrational modes of both the molecule and the surface [8,23,34,35]. However, the calculated vibrational lifetimes are larger than experimental values [23,33]. It should be noted that the dephasing process was described either in terms of the exchange model based on the thermal excitation of another vibrational mode localized at the adsorbed molecule [36], or in terms of elastic scattering of the substrate phonons at the adsorbed molecule [35]. It is worth mentioning that a cross term between these two processes was emphasized in the description of the photodesorption kinetics [37]. In addition, theoretical descriptions of phonon-induced dephasing of the internal vibrational mode of diatomic molecules, say the V mode [38], as well as of the perpendicular adsorbate-surface vibrational mode, say the T mode [39–41], were made. For a whole molecule, vibrating normal to the surface in the top position of an atom of the substrate, it was demonstrated that the contribution of the modes vibrating perpendicularly to the surface makes a negligible contribution to the line shape [41]. The evaluation of the phonon spectra clearly shows that the line shape is dominated by dephasing due to vibrations parallel to the surface.

More recently, by introducing an additional infrared pump beam, it became possible to study the dynamical processes involving the hot band of the spectra. Here the molecule initially populated by an infrared pump pulse is ultimately tested by two coincident infrared and visible probe pulses. Due to the possible overlapping of the pulses, the nonlinear process underlying the polarization created in the molecule is really a five-wave-mixing process involving the characteristic sequential, self-modulation, and interference terms. By using this pumped infrared-visible sum-frequency generation (PSFG) spectroscopic method, the anharmonicity of the Si-H stretching mode of H/Si(111)-(1×1) was determined [42]. For infrared-visible PSFG experiments, quantities like the recovery time of the ground-state population of either the Si-H stretching mode of the H/Si(111)-(1×1) surface [9,10] or the C-H stretching mode of the H/C(111)-(1×1) surface [43,44], as well as the vibrational energy relaxation of the C-H stretching mode of methyl thiolate adsorbed on a metallic surface [45–47], were experimentally determined. In a recent theoretical study on surface vibrational infrared-visible sum-frequency generation spectroscopy applied to adsorbed molecules [48], frequency and time dependences of physical observables were evaluated on the basis of Gaussian light pulses whose durations are supposed to be longer than any dephasing times. The recovery time and time dependence of the transient SFG signals were evaluated for experimental situations where the infrared probe beam was resonant with either the first or second vibrational transitions. From the detailed steady-state and time-dependent analysis presented here, the different contributions are evaluated, and the influence of the vibrational and electronic dephasings are analyzed.

The paper is organized as follows. In Sec. II, we recall the description of the general time evolution required for five-wave mixing in Markovian systems. This is based on an evaluation of the multiple time integral valid for Lorentzian pulses, as well as on the spectral decomposition of the evolution Liouvillians. The second- and fourth-polarization terms, previously evaluated in the steady-state analysis of the dip in the PSFG absorption spectra, are introduced briefly. Next, in Sec. III, terms which give the dominant contribution in the infrared-visible PSFG, enable us to evaluate the time-integrated signal. Two different situations are discussed depending on whether the infrared probe beam is resonant with the first or second vibrational transition. By adopting these particular resonant conditions, we show that the integrated PSFG signal is very sensitive to the specific pure vibrational dephasing processes acting on the vibrational transition resonantly excited.

II. GENERAL TIME EVOLUTION AND POLARIZATION

A sum-frequency generation is a three-wave-mixing process. Now, if an additional pump laser is applied to the adsorbate system, then the subsequent pumped sum-frequency generation process occurring on the adsorbate is really a five-wave-mixing process. With respect to the usual infrared-visible SFG experiments, the additional infrared pump beam generates a population in the vibrationally excited states of the ground electronic configuration, which is later tested by the infrared and visible probe beams. This is the physical picture supported by the sequential term contributing to the PSFG signal in the steady-state regime [49]. The contribution of the self-modulation term is quite similar, except that pumping and probing in the infrared range are done by the same infrared probe beam. Of course, other contributions, like the synchronous and asynchronous interfering terms, cannot be interpreted this way due to the alternation of the interacting infrared beams. Note that for time-resolved PSFG, there is no way to analyze these contributions separately, since we are dealing with the intensity and not with the polarization. In typical PSFG experiments [43–48], the infrared pump and probe beams, as well as the visible probe beam, are collimated in three different directions, as shown in Fig. 1. Nevertheless, if we are interested in detecting the sum-frequency signal in the direction $\vec{k}_{\mathrm{ir}}+\vec{k}_{\mathrm{vis}}$, corresponding to the sum of the infrared and visible probe beam wave vectors, the wave vector of the infrared pump beam does not participate to the phase-matching conditions. For this reason, one important peculiarity of the pumped sum-frequency generation experiments lies in the fact that both second- and fourth-order polarization terms, contribute to the detected

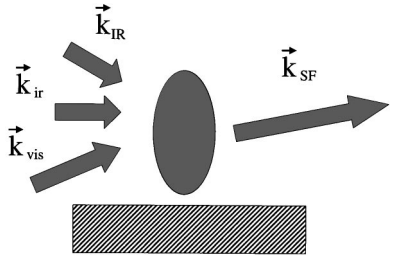

FIG. 1. Experimental geometry required in a pumped SFG experiment to avoid additional contributions.

sum-frequency signal intensity, so that

$$I_{SFG}(t) \propto |\vec{P}^{(2)}(\vec{k}_{SF},t) + \vec{P}^{(4)}(\vec{k}_{SF},t)|^2. \tag{2.1}$$

The required second- and fourth-polarization terms $\vec{P}^{(n)}(\vec{k}_{SF},t) = \mathrm{Tr}[\rho^{(n)}(\vec{k}_{SF},t)\vec{\mu}]$, $n=2$ and 4, are straightforwardly deduced from the perturbational expansion of the density matrix valid for weak excitation light beams. The evolution Liouvillian $G(t-\tau) = \exp[(-i/\hbar)(L_0 - i\hbar\Gamma)(t-\tau)]$ is expressed along the same lines previously introduced in the dephasing analysis on the dip structure of the PSFG absorption spectrum. As usual, L_0 is the zero-order Liouvillian built from the Hamiltonian of the molecular adsorbate alone, and Γ is the damping operator. Notice that the pure dephasing constants $\Gamma_{ij}^{(d)}$ are related to the dephasing constants Γ_{ijij} by the usual relation $\Gamma_{ijij} = 1/2[\Gamma_{iiii} + \Gamma_{jjjj}] + \Gamma_{ij}^{(d)}$, where the Γ_{uuuu} are the total decay rates of levels $u = i,j$. Here, special attention will be paid to the pure vibrational dephasing occurring in the vibrational structure of the ground electronic configuration and induced by the surface. For our purpose, a convenient model of the adsorbed system can be made of two electronic configurations and of the vibrational bonding mode, say the C-H or Si-H mode interacting with the infrared pump and probe beams, in most of the cited

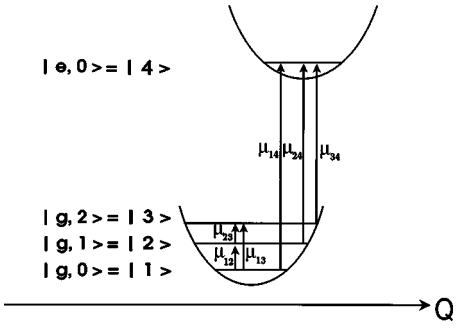

FIG. 2. Representation of the model introduced for the adsorbed system. Q is the bonding coordinate between the adsorbed system and the surface. The two parabola stand for the ground and first excited electronic configurations. Their corresponding vibrational energies are different because of anharmonicity, and are given by $\omega_{21} = 2838\ \mathrm{cm}^{-1}$ and $\omega_{32} = 2736\ \mathrm{cm}^{-1}$. The electronic transition energy is set equal to $\omega_{41} = 30\,000\ \mathrm{cm}^{-1}$. The dipole moments are chosen real, and their modulus corresponds to $\mu_{12} = \mu_{14} = \mu_{24} = \mu_{34}$, while $\mu_{23} = 1.5\mu_{12}$. The dephasing constants are given by $\Gamma_{1313} = 30\ \mathrm{cm}^{-1}$, $\Gamma_{1414} = 30\ \mathrm{cm}^{-1}$, $\Gamma_{2323} = 15.5\ \mathrm{cm}^{-1}$, $\Gamma_{2424} = 40\ \mathrm{cm}^{-1}$, and $\Gamma_{3434} = 30\ \mathrm{cm}^{-1}$.

experiments. This model is shown in Fig. 2. At low temperature, only the first three vibrational states of the ground electronic configuration are required for the dynamics participating to the five-wave-mixing process, while the excited electronic configuration is kept vibrationally unexcited due to the nonresonant condition always satisfied by the visible probe beam. Finally, $L_V(t)$ is the interaction Liouvillian associated with the interaction between the laser beams and the molecular adsorbates. While the infrared pump beam has a fixed frequency and is chosen resonant with the first vibrational transition frequency ω_{21}, as shown in Fig. 2, the infrared probe beam is usually scanned around the first and the second vibrational transition frequencies ω_{21} and ω_{32}. These different types of excitation will enable a clear distinction of the pure dephasing processes acting on the different vibrational transitions. Note that ω_{32} can differ from ω_{21} because of anharmonicity. Finally, for the sake of simplicity, the visible beam frequency is chosen to be strongly nonresonant with the electronic transition, so that the Placzek approximation can be used [50]. As a consequence, the rotating-wave approximation will be valid for the interaction between the adsorbed molecule and the infrared pump and probe beams, only. Therefore, the interaction term $V(t)$ takes the form

$$\begin{aligned} V_{mn}(t) = -\langle m|\vec{\mu}|n\rangle \cdot \Big[& \vec{E}(\sigma_{mn}\omega_{IR}) \\ & \times e^{-i\sigma_{mn}(\omega_{IR}t - \vec{k}_{IR}\cdot\vec{r})}\mathcal{L}_{IR}(t) \\ & + \vec{E}(\sigma_{mn}\omega_{ir}) e^{-i\sigma_{mn}(\omega_{ir}t - \vec{k}_{ir}\cdot\vec{r})}\mathcal{L}_{ir}(t) \\ & + \sum_{s=\pm 1} \vec{E}(s\omega_{vis}) e^{-is(\omega_{vis}t - \vec{k}_{vis}\cdot\vec{r})}\mathcal{L}_{vis}(t) \Big], \end{aligned} \tag{2.2}$$

where ω_p, $\vec{k}_p$, and $\mathcal{L}_p(t)$ are the frequencies, wave vectors, and laser pulse shapes of the infrared pump ($p = \mathrm{IR}$), infrared probe ($p = \mathrm{ir}$), and visible probe ($p = \mathrm{vis}$) pulses. Also, the symbol σ_{mn} is equal to $+1$ or -1, depending on whether the energy gap between the states $|m\rangle$ and $|n\rangle$, corresponding to $(E_m - E_n)$, is positive or negative, respectively. The pulse shapes are choosen as $\mathcal{L}_j(t) = e^{-\gamma_j|t_j - t|}$ where $\overline{t_j}$ represents the pumping or probing times and $T_j = \gamma_j^{-1}$ the corresponding pumping or probing pulse durations, depending on the nature of the field j.

As mentioned earlier, in a PSFG experiment the second- and fourth-order polarization terms contribute to the phase-matched signal. Therefore, we are left with the evaluation of $\vec{P}^{(2)}(\vec{k}_{SF},t)$ and $\vec{P}^{(4)}(\vec{k}_{SF},t)$. To study the required dynamical evolution of the adsorbate bonding mode, the four-level model presented in Fig. 2 is perfectly convenient. Note that this model previously proved very useful in analyzing the influence of the pure vibrational and electronic dephasings on the dip observed in the PSFG absorption spectra of molecular adsorbates [49].

As long as we are concerned by a Markovian dynamical system, the contribution of the second-order polarization

term, associated with a given pathway η, can be formally expressed as

$$\vec{P}_{\eta}^{(2)}(\mathrm{ir,vis},\vec{k}_{\mathrm{SF}},t)=\left(-\frac{i}{\hbar}\right)^2\vec{S}_{\eta}^{(2)}e^{s_{\eta}^{(2)}t}e^{i\vec{k}_{\mathrm{SF}}\cdot\vec{r}}\times\int_{-\infty}^{t}dt_2e^{B_{\eta}^{(2)}t_2}e^{-\gamma_j|t_2-\bar{t}_j|}\times\int_{-\infty}^{t_2}dt_1e^{A_{\eta}^{(2)}t_1}e^{-\gamma_i|t_1-\bar{t}_i|},\quad(2.3)$$

where the constants $A_{\eta}^{(2)}$, $B_{\eta}^{(2)}$, $S_{\eta}^{(2)}$, and $s_{\eta}^{(2)}$ are listed in Ref. [49], and correspond to a system initially thermalized, $\rho(-\infty)=|1\rangle\langle 1|$. Note that like in a traditional sum-frequency experiment, there is no infrared pump beam acting on the adsorbed molecule for this contribution. In addition, due to the initial conditions and the particular situation of a nonresonant visible beam, the main contribution involves processes where the infrared beam interacts first, only. Once the integration constants have been introduced, the second-order polarization in the direction $\vec{k}_{\mathrm{SF}}$ results in the form

$$\vec{P}^{(2)}(\vec{k}_{\mathrm{SF}},t)=\sum_{\eta}\vec{P}_{\eta}^{(2)}(\mathrm{ir,vis};\vec{k}_{\mathrm{SF}},t)=\sum_{\eta}\vec{S}_{\eta}^{(2)}e^{s_{\eta}^{(2)}t}e^{i\vec{k}_{\mathrm{SF}}\cdot\vec{r}}\times\left[\sum_{\beta=1}^{7}H(t-\tau_{\beta\eta}^{>})D_{\beta\eta}^{>}e^{d_{\beta\eta}^{>}t}+\bar{H}(\tau_{1\eta}^{<}-t)D_{1\eta}^{<}e^{d_{1\eta}^{<}t}+\sum_{\beta=1}^{6}H(t-\tau_{1,\beta\eta}^{\times})\bar{H}(\tau_{2,\beta\eta}^{\times}-t)D_{\beta\eta}^{\times}e^{d_{\beta\eta}^{\times}t}\right].\quad(2.4)$$

This expression is completely general, and is valid for steady-state or pulsed experiments, as long as we are dealing with Markovian systems. Note that for second-order terms, only coherences participate in the dynamical evolution. For this reason the evaluation of the contributions associated with the two different pathways is quite easy.

The evaluation of the fourth-order term is evaluated similarly. Again, the contribution for a given pathway η and a particular combination of fields (I, J, K, L), satisfying the phase-matched condition, is given by the formal expression

$$\vec{P}_{\eta}^{(4)}(I,J,K,L;\vec{k}_{\mathrm{SF}},t)=\left(-\frac{i}{\hbar}\right)^4\vec{S}_{\eta}^{(4)}e^{s_{\eta}^{(4)}t}\int_{-\infty}^{t}dt_4e^{D_{\eta}^{(4)}t_4}e^{-\gamma_l|t_4-\bar{t}_l|}\int_{-\infty}^{t_4}dt_3e^{C_{\eta}^{(4)}t_3}e^{-\gamma_k|t_3-\bar{t}_k|}\times\int_{-\infty}^{t_3}dt_2e^{B_{\eta}^{(4)}t_2}e^{-\gamma_j|t_2-\bar{t}_j|}\int_{-\infty}^{t_2}dt_1e^{A_{\eta}^{(4)}t_1}e^{-\gamma_i|t_1-\bar{t}_i|},\quad(2.5)$$

where the constants associated with the various pathways have been evaluated in our previous work [49]. Therefore, the fourth-order polarization in the direction $\vec{k}_{\mathrm{SF}}$ takes the form

$$\vec{P}^{(4)}(I,J,K,L;\vec{k}_{\mathrm{SF}},t)=\sum_{\xi=1}^{35}\vec{P}_{\xi}^{(4)}(I,J,K,L;\vec{k}_{\mathrm{SF}},t)=\sum_{\xi=1}^{35}\vec{S}_{\xi}^{(4)}e^{s_{\xi}^{(4)}t}e^{i\vec{k}_{\mathrm{SF}}\cdot\vec{r}}\left[\sum_{\nu=1}^{141}H(t-\lambda_{\nu\xi}^{>})Q_{\nu\xi}^{>}e^{q_{\nu\xi}^{>}t}+\bar{H}(\lambda_{1\xi}^{<}-t)Q_{1\xi}^{<}e^{q_{1\xi}^{<}t}+\sum_{\nu=1}^{220}H(t-\lambda_{1,\nu\xi}^{\times})\bar{H}(\lambda_{2,\nu\xi}^{\times}-t)Q_{\nu\xi}^{\times}e^{q_{\nu\xi}^{\times}t}\right].\quad(2.6)$$

In addition, because of the overlapping between the various light pulses, their interactions with the adsorbed system can take place with different chronological orders. They correspond to the various combinations of the subscripts I, J, K, and L taken from the three different fields and participating in the five-wave-mixing process. For the sake of simplicity, the field indices have not been reported in all the constants. They will be introduced if required. Note that these combinations generate four different types of contributions termed the sequential term, the self-modulation term, and the synchronous and asynchronous interference terms, as discussed previously [48,49].

III. TIME DEPENDENCE OF PUMPED SUM-FREQUENCY GENERATION SIGNAL

In Sec. II, we evaluated the second-and fourth-order terms contributing to the $\vec{k}_{\mathrm{SF}}$ component of the polarization. For the usual time-resolved PSFG experiment, the physical observable is the time integrated signal given by the expression

$$I_{\mathrm{SFG}}(\Delta_{\text{ir-IR}}\Delta_{\text{ir-vis}})=\int_{-\infty}^{+\infty}dt|P^{(2)}(\vec{k}_{\mathrm{SF}},t)+P^{(4)}(\vec{k}_{\mathrm{SF}},t)|^2,\quad(3.1)$$

where the symbol $\Delta_{\text{ir-IR}}=\overline{t}_{\text{tr}}-\overline{t}_{\text{IR}}$ stands for the time of delay between the infrared pump and the infrared probe pulses, while $\Delta_{\text{ir-vis}}=\overline{t}_{\text{ir}}-\overline{t}_{\text{vis}}$ stands for the infrared and visible probe pulses. Note that the PSFG experiments performed right now were made with coincident infrared and visible probe pulses, so that $\Delta_{\text{ir-vis}}=0$. The introduction of this parameter will offer, in the future, new opportunities for the determination of the dephasing constants in the vibrationally excited states.

As mentioned above the integrated signal in the $\vec{k}_{\text{SF}}$ direction involves three different types of terms

$$I_{\text{SFG}}(\vec{k}_{\text{SF}},\Delta_{\text{ir-IR}},\Delta_{\text{ir-vis}}) = I^{(2)}_{\text{SFG}}(\vec{k}_{\text{SF}},\Delta_{\text{ir-vis}}) + I^{(4)}_{\text{SFG}}(\vec{k}_{\text{SF}},\Delta_{\text{ir-IR}},\Delta_{\text{ir-vis}}) + I^{(2\text{-}4)}_{\text{SFG}}(\vec{k}_{\text{SF}},\Delta_{\text{ir-IR}},\Delta_{\text{ir-vis}}). \tag{3.2}$$

The first contribution comes from the second-order background SFG polarization. With the additional notations, $I(A,\tau)=e^{A\tau}/A$ and $J(A;\tau_1,\tau_2)=(e^{A\tau_1}-e^{A\tau_2})/A$, as well as $(\tau_1,\tau_2)_{\text{inf}}$ or $(\tau_1,\tau_2)_{\text{sup}}$, standing for the lower or higher terms involved in the brackets, we have

$$\begin{aligned}
I^{(2)}_{\text{SFG}}(\vec{k}_{\text{SF}},\Delta_{\text{ir-vis}}) = \sum_{\eta=1}^{2}\sum_{\eta'=1}^{2} S^{(2)}_{\eta}S^{(2)*}_{\eta'}\Bigg[&-\sum_{\beta=1}^{7}\sum_{\beta'=1}^{7} D^{>}_{\beta\eta}D^{>*}_{\beta'\eta'}I(s^{(2)}_{\eta}+s^{(2)*}_{\eta'}+d^{>}_{\beta\eta}+d^{>*}_{\beta'\eta'};(\tau^{>}_{\beta\eta},\tau^{>}_{\beta'\eta'})_{\text{sup}}) \\
&+D^{<}_{1\eta}D^{<*}_{1\eta'}I(s^{(2)}_{\eta}+s^{(2)*}_{\eta'}+d^{<}_{1\eta}+d^{<*}_{1\eta'};(\tau^{<}_{1\eta},\tau^{<}_{1\eta'})_{\text{inf}}) \\
&+\sum_{\beta=1}^{6}\sum_{\beta'=1}^{6} D^{\times}_{\beta\eta}D^{\times*}_{\beta'\eta'}H((\tau^{\times}_{2,\beta\eta},\tau^{\times}_{2,\beta'\eta'})_{\text{inf}}-(\tau^{\times}_{1,\beta\eta},\tau^{\times}_{1,\beta'\eta'})_{\text{sup}}) \\
&\times J(s^{(2)}_{\eta}+s^{(2)*}_{\eta'}+d^{\times}_{\beta\eta}+d^{\times*}_{\beta'\eta'};(\tau^{\times}_{2,\beta\eta},\tau^{\times}_{2,\beta'\eta'})_{\text{inf}},(\tau^{\times}_{1,\beta\eta},\tau^{\times}_{1,\beta'\eta'})_{\text{sup}})\Bigg] \\
+2\,\text{Re}\Bigg\{\sum_{\eta=1}^{2}\sum_{\eta'=1}^{2} S^{(2)}_{\eta}S^{(2)*}_{\eta'}\Bigg[&\sum_{\beta=1}^{7} D^{>}_{\beta\eta}D^{<*}_{1\eta'}\overline{H}(\tau^{<}_{1\eta'}-\tau^{>}_{\beta\eta})J(s^{(2)}_{\eta}+s^{(2)*}_{\eta'}+d^{>}_{\beta\eta}+d^{<*}_{1\eta'};\tau^{<}_{1\eta'},\tau^{>}_{\beta\eta}) \\
&+\sum_{\beta=1}^{7}\sum_{\beta'=1}^{6} D^{>}_{\beta\eta}D^{\times*}_{\beta'\eta'}\overline{H}(\tau^{\times}_{2,\beta'\eta'}-(\tau^{>}_{\beta\eta},\tau^{\times}_{1,\beta'\eta'})_{\text{sup}}) \\
&\times J(s^{(2)}_{\eta}+s^{(2)*}_{\eta'}+d^{>}_{\beta\eta}+d^{\times*}_{\beta'\eta'};\tau^{\times}_{2,\beta'\eta'},(\tau^{>}_{\beta\eta},\tau^{\times}_{1,\beta'\eta'})_{\text{sup}}) \\
&+\sum_{\beta'=1}^{6} D^{<}_{1\eta}D^{\times*}_{\beta'\eta'}\overline{H}((\tau^{<}_{1\eta},\tau^{\times}_{2,\beta'\eta'})_{\text{inf}}-\tau^{\times}_{1,\beta'\eta'})J(s^{(2)}_{\eta}+s^{(2)*}_{\eta'}+d^{<}_{1\eta}+d^{\times*}_{\beta'\eta'};(\tau^{<}_{1\eta},\tau^{\times}_{2,\beta'\eta'})_{\text{inf}},\tau^{\times}_{1,\beta'\eta'})\Bigg]\Bigg\}.
\end{aligned} \tag{3.3}$$

The second contribution comes from the fourth-order polarization term. It involves the sequential and interfering terms which come from the fact that the adsorbed system experiences pump and probe beams, as well as the self-modulation term which comes from the probe beams only. Because the various possible ordering of the interacting fields must be accounted for, we have to introduce the sums over the various combinations of fields noted $\mathcal{C}_i$ and $\mathcal{C}'_i$. Therefore, the corresponding contribution takes the form

$$\begin{aligned}
I^{(4)}_{\text{SFG}}(\vec{k}_{\text{SF}},\Delta_{\text{ir-IR}},\Delta_{\text{ir-vis}}) = &\sum_{\mathcal{C}_i=1}^{4}\sum_{\mathcal{C}'_i=1}^{4}\sum_{\xi=1}^{16}\sum_{\xi'=1}^{16} \\
&\times\Bigg\{ S^{(4)}_{\xi}S^{(4)*}_{\xi'}\Bigg[-\sum_{\nu=1}^{141}\sum_{\nu'=1}^{141} Q^{>}_{\nu\xi}Q^{>*}_{\nu'\xi'}I(s^{(4)}_{\xi}+s^{(4)*}_{\xi'}+q^{>}_{\nu\xi}+q^{>*}_{\nu'\xi'};(\lambda^{>}_{\nu\xi},\lambda^{>}_{\nu'\xi'})_{\text{sup}}) \\
&+Q^{<}_{1\xi}Q^{<*}_{1\xi'}I(s^{(4)}_{\xi}+s^{(4)*}_{\xi'}+q^{<}_{1\xi}+q^{<*}_{1\xi'};(\lambda^{<}_{1\xi},\lambda^{<}_{1\xi'})_{\text{inf}}) \\
&+\sum_{\nu=1}^{220}\sum_{\nu'=1}^{220} Q^{\times}_{\nu\xi}Q^{\times*}_{\nu'\xi'}H((\lambda^{\times}_{2,\nu\xi},\lambda^{\times}_{2,\nu'\xi'})_{\text{inf}}-(\lambda^{\times}_{1,\nu\xi},\lambda^{\times}_{1,\nu'\xi'})_{\text{sup}})
\end{aligned}$$

$$\times J(s_{\xi}^{(4)}+s_{\xi'}^{(4)*}+q_{\nu\xi}^{\times}+q_{\nu'\xi'}^{\times *};(\lambda_{2,\nu\xi}^{\times},\lambda_{2,\nu'\xi'}^{\times})_{\inf},(\lambda_{1,\nu\xi}^{\times},\lambda_{1,\nu'\xi'}^{\times})_{\sup})\Bigg]$$

$$+2\,\mathrm{Re}\Bigg\{S_{\xi}^{(4)}S_{\xi'}^{(4)*}\Bigg[\sum_{\nu=1}^{141}Q_{\nu\xi}^{>}Q_{1\xi'}^{<*}\overline{H}(\lambda_{1\xi'}^{<}-\lambda_{\nu\xi}^{>})J(s_{\xi}^{(4)}+s_{\xi'}^{(4)*}+q_{\nu\xi}^{>}+q_{1\xi'}^{<*};\lambda_{1\xi'}^{<},\lambda_{\nu\xi}^{>})$$

$$+\sum_{\nu=1}^{141}\sum_{\nu'=1}^{220}Q_{\nu\xi}^{>}Q_{\nu'\xi'}^{\times *}\overline{H}(\lambda_{2,\nu'\xi'}^{\times}-(\lambda_{\nu\xi}^{>},\lambda_{1,\nu'\xi'}^{\times})_{\sup})$$

$$\times J(s_{\xi}^{(4)}+s_{\xi'}^{(4)*}+q_{\nu\xi}^{>}+q_{\nu'\xi'}^{\times *};\lambda_{2,\nu'\xi'}^{\times},(\lambda_{\nu\xi}^{>},\lambda_{1,\nu'\xi'}^{\times})_{\sup})$$

$$+\sum_{\nu'=1}^{220}Q_{1\xi}^{<}Q_{\nu'\xi'}^{\times *}\overline{H}((\lambda_{1\xi}^{<},\lambda_{2,\nu'\xi'}^{\times})_{\inf}-\lambda_{1,\nu'\xi'}^{\times})$$

$$\times J(s_{\xi}^{(4)}+s_{\xi'}^{(4)*}+q_{1\xi}^{<}+q_{\nu'\xi'}^{\times *};(\lambda_{1\xi}^{<},\lambda_{2,\nu'\xi'}^{\times})_{\inf},\lambda_{1,\nu'\xi'}^{\times})\Bigg]\Bigg\}\Bigg\}. \tag{3.4}$$

Here the various combinations are for the sequential term ($\mathcal{C}_{seq}\equiv\{I=\mathrm{IR},J=\mathrm{IR},K=\mathrm{ir},L=\mathrm{vis}\}$), for the self-modulated term ($\mathcal{C}_{\text{self-mod}}\equiv\{I=\mathrm{ir},J=\mathrm{ir},K=\mathrm{ir},L=\mathrm{vis}\}$), and for the interfering terms ($\mathcal{C}_{\text{synch.int.}}\equiv\{I=\mathrm{ir},J=\mathrm{IR},K=\mathrm{IR},L=\mathrm{vis}\},\mathcal{C}_{\text{asynch.int.}}\equiv\{I=\mathrm{IR},J=\mathrm{ir},K=\mathrm{IR},L=\mathrm{vis}\}$). Finally, the third and last contribution corresponds to an interfering term between the second-order background SFG polarization and the fourth-order SFG polarization of the pumped system. It is given by the expression

$$I_{\mathrm{SFG}}^{(2\text{-}4)}(\vec{k}_{\mathrm{SF}},\Delta_{\text{ir-IR}},\Delta_{\text{ir-vis}})=2\,\mathrm{Re}\Bigg\{\sum_{\mathcal{C}_i=1}^{4}\sum_{\eta=1}^{2}\sum_{\xi=1}^{16}S_{\eta}^{(2)}S_{\xi}^{(4)*}$$

$$\times\Bigg[-\sum_{\beta=1}^{7}\sum_{\nu=1}^{141}D_{\beta\eta}^{>}Q_{\nu\xi}^{>*}I(s_{\eta}^{(2)}+s_{\xi}^{(4)*}+d_{\beta\eta}^{>}+q_{\nu\xi}^{>*};(\tau_{\beta\eta}^{>},\lambda_{\nu\xi}^{>})_{\sup})$$

$$+D_{1\eta}^{<}Q_{1\xi}^{<*}I(s_{\eta}^{(2)}+s_{\xi}^{(4)*}+d_{1\eta}^{<}+q_{1\xi}^{<*};(\tau_{1\eta}^{<},\lambda_{1\xi}^{<})_{\inf})$$

$$+\sum_{\beta=1}^{6}\sum_{\nu=1}^{220}D_{\beta\eta}^{\times}Q_{\nu\xi}^{\times *}H((\tau_{2,\beta\eta}^{\times},\lambda_{2,\nu\xi}^{\times})_{\inf}-(\tau_{1,\beta\eta}^{\times},\lambda_{1,\nu\xi}^{\times})_{\sup})$$

$$\times J(s_{\eta}^{(2)}+s_{\xi}^{(4)*}+d_{\beta\eta}^{\times}+q_{\nu\xi}^{\times *};(\tau_{2,\beta\eta}^{\times},\lambda_{2,\nu\xi}^{\times})_{\inf},(\tau_{1,\beta\eta}^{\times},\lambda_{1,\nu\xi}^{\times})_{\sup})$$

$$+\sum_{\beta=1}^{7}D_{\beta\eta}^{>}Q_{1\xi}^{<*}\overline{H}(\lambda_{1\xi}^{<}-\tau_{\beta\eta}^{>})J(s_{\eta}^{(2)}+s_{\xi}^{(4)*}+d_{\beta\eta}^{>}+q_{1\xi}^{<*};\lambda_{1\xi}^{<},\tau_{\beta\eta}^{>})$$

$$+\sum_{\beta=1}^{7}\sum_{\nu=1}^{220}D_{\beta\eta}^{>}Q_{\nu\xi}^{\times *}\overline{H}(\lambda_{2,\nu\xi}^{\times}-(\tau_{\beta\eta}^{>},\lambda_{1,\nu\xi}^{\times})_{\sup})J(s_{\eta}^{(2)}+s_{\xi}^{(4)*}+d_{\beta\eta}^{>}+q_{\nu\xi}^{\times *};\lambda_{2,\nu\xi}^{\times},(\tau_{\beta\eta}^{>},\lambda_{1,\nu\xi}^{\times})_{\sup})$$

$$+\sum_{\nu=1}^{141}D_{1\eta}^{<}Q_{\nu\xi}^{>*}\overline{H}(\tau_{1\eta}^{<}-\lambda_{\nu\xi}^{>})J(s_{\eta}^{(2)}+s_{\xi}^{(4)*}+d_{1\eta}^{<}+q_{\nu\xi}^{>*};\tau_{1\eta}^{<},\lambda_{\nu\xi}^{>})$$

$$+\sum_{\nu=1}^{220}D_{1\eta}^{<}Q_{\nu\xi}^{\times *}H((\tau_{1\eta}^{<},\lambda_{2,\nu\xi}^{\times})_{\inf}-\lambda_{1,\nu\xi}^{\times})J(s_{\eta}^{(2)}+s_{\xi}^{(4)*}+d_{1\eta}^{<}+q_{\nu\xi}^{\times *};(\tau_{1\eta}^{<},\lambda_{2,\nu\xi}^{\times})_{\inf},\lambda_{1,\nu\xi}^{\times})$$

$$+\sum_{\beta=1}^{6}\sum_{\nu=1}^{141}D_{\beta\eta}^{\times}Q_{\nu\xi}^{>*}H(\tau_{2,\beta\eta}^{\times}-(\tau_{1,\beta\eta}^{\times},\lambda_{\nu\xi}^{>})_{\sup})J(s_{\eta}^{(2)}+s_{\xi}^{(4)*}+d_{\beta\eta}^{\times}+q_{\nu\xi}^{>*};\tau_{2,\beta\eta}^{\times},(\tau_{1,\beta\eta}^{\times},\lambda_{\nu\xi}^{>})_{\sup})$$

$$+\sum_{\beta=1}^{6}D_{\beta\eta}^{\times}Q_{1\xi}^{<*}H((\tau_{2,\beta\eta}^{\times},\lambda_{1\xi}^{<})_{\inf}-\tau_{1,\beta\eta}^{\times})J(s_{\eta}^{(2)}+s_{\xi}^{(4)*}+d_{\beta\eta}^{\times}+q_{1\xi}^{<*};(\tau_{2,\beta\eta}^{\times},\lambda_{1\xi}^{<})_{\inf},\tau_{1,\beta\eta}^{\times})\Bigg]\Bigg\}. \tag{3.5}$$

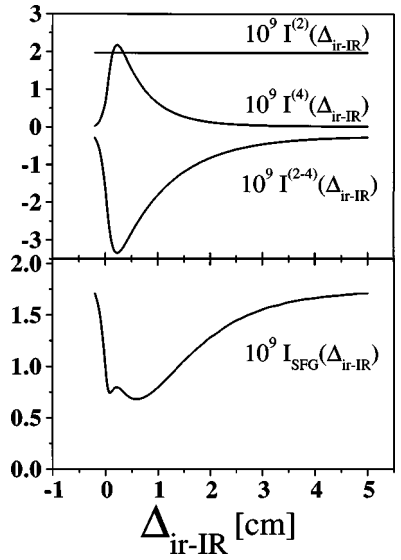

FIG. 3. Representation of the time-resolved profile as a function of the pump-probe time of delay, for infrared field frequencies equal to the first vibrational transition $\omega_{IR}=\omega_{IR}=\omega_{21}=2838\,cm^{-1}$ and $\omega_{vis}=20\,000\,cm^{-1}$. The spectral widths are $\gamma_{IR}=15\,cm^{-1}$, $\gamma_{ir}=12\,cm^{-1}$, and $\gamma_{vis}=10\,cm^{-1}$. The corresponding total decay rates are given by $\Gamma_{2222}=0.1\,cm^{-1}$, $\Gamma_{3333}=1\,cm^{-1}$, and $\Gamma_{4444}=1\,cm^{-1}$, while the pure dephasing constants are $\Gamma^{(d)}_{1212}=1\,cm^{-1}$, $\Gamma^{(d)}_{2323}=3\,cm^{-1}$, and $\Gamma^{(d)}_{i4i4}=5\,cm^{-1}\,\forall$, $i=1$, 2, and 3. In the upper part of the figure, we show the three different contributions $I^{(2)}_{SFG}(\vec{k}_{SF},\Delta_{ir\text{-}vis})$, $I^{(4)}_{SFG}(\vec{k}_{SF},\Delta_{ir\text{-}IR},\Delta_{ir\text{-}vis})$, and $I^{(2\text{-}4)}_{SFG}(\vec{k}_{SF},\Delta_{ir\text{-}IR},\Delta_{ir\text{-}vis})$, which contribute to the total intensity. The amplitudes of the fields correspond to $E(\omega_{ir})=E(\omega_{vis})=0.1\times E(\omega_{IR})$.

Of course, all the constants depend on the fields participating in a given combination. For the sake of simplicity, their indices have been omitted here. We have determined a general expression for the time-integrated signal obtained for an infrared-visible PSFG experiment. Therefore, Eqs. (3.3)–(3.5) will be the starting point of a number of numerical simulations to emphasize the role of the possible vibrational dephasing processes taking place on adsorbed molecules. Only the case of coincident infrared and visible probe pulses, $\Delta_{ir\text{-}vis}=0$, will be considered here. All along, the vibrational transition frequencies correspond to $\omega_{21}=2838\,cm^{-1}$ and $\omega_{32}=2736\,cm^{-1}$ and the electronic transition frequency is chosen as $\omega_{41}=30\,000\,cm^{-1}$. The values of all the physical parameters are typical values taken from experimental situations like H on Si(111) or H on C(111).

We first analyze the influence of the physical parameters involving lifetimes, dephasing times, and amplitudes of the fields time dipole moments. In the first simulation, we represent the variations of the integrated PSFG signal versus the time of delay between the infrared pump pulse and the coincident infrared and visible probe pulses. This is shown in Fig. 3, where the time-resolved profile is evaluated for infrared pump and infrared probe fields exactly resonant with the first vibrational transition $|1\rangle\leftrightarrow|2\rangle$. This implies that $\omega_{IR}=\omega_{ir}=\omega_{21}$. In the low part of this figure, we show the time dependence of the total intensity $I_{SFG}(\Delta_{ir\text{-}IR})$, while in the upper part we draw the individual contributions associated with the second-order $I^{(2)}_{SFG}(\Delta_{ir\text{-}IR})$ and fourth-order $I^{(4)}_{SFG}(\Delta_{ir\text{-}IR})$ contributions as well as mixed second- and fourth-order $I^{(2\text{-}4)}_{SFG}(\Delta_{ir\text{-}IR})$ contributions. Except the small peak appearing in the vicinity of the minimum, we observe at short times a decrease of the total integrated PSFG signal. This results from a depopulation of the ground state induced by the pump pulse, and occurring with a characteristic time corresponding to the duration of the pump pulse. At long times, the excited state $|2\rangle$ begins to relax at the benefit of the ground-state population. This recovery of the ground-state population, which evolves mainly with the lifetime Γ^{-1}_{2222}, promotes the SFG process, which recovers its initial efficiency at long times, as can be seen from this figure. Besides this overall feature, the small peak observed near the minimum of the curve comes from the fact that the various contributions to the signal intensity do not have the same time dependence. The contribution $I^{(4)}_{SFG}(\vec{k}_{SF},\Delta_{ir\text{-}IR},\Delta_{ir\text{-}vis})$ depends on $\vec{P}^{(4)}(\vec{k}_{SF},t)$ only, while $I^{(2\text{-}4)}_{SFG}(\vec{k}_{SF},\Delta_{ir\text{-}IR},\Delta_{ir\text{-}vis})$ depends simultaneously on $\vec{P}^{(2)}(\vec{k}_{SF},t)$ and $\vec{P}^{(4)}(\vec{k}_{SF},t)$. Note that $\vec{P}^{(2)}(\vec{k}_{SF},t)$ is only a function of the dephasing times Γ^{-1}_{1212} since the visible field is strongly nonresonant, while $\vec{P}^{(4)}(\vec{k}_{SF},t)$ depends on the dephasing times Γ^{-1}_{1212} and Γ^{-1}_{2323}, but also on the lifetime Γ^{-1}_{2222}. Because these last two terms do not have the same dependence on the relaxation and dephasing times, their corresponding time-resolved profiles are different, as can be seen from the upper part of the figure. The sum of these contributions having different time dependences results in a small peak in the vicinity of the minimum where the time variations are rapid. Another important aspect of the time-dependent PSFG signal intensity results from the fact that various processes contribute to the polarization terms. Because different combinations of fields contribute to the sequential, self-modulation, and interfering terms, their contributions to the intensity will be strongly influenced by the relative amplitude of the fields. This is unusual in nonlinear optics, where we are often concerned with the contribution of a single process leaving the field amplitudes as simple multiplicative constants. Moreover, here the PSFG signal mixes the second- and fourth-order contributions, and the influence of the pump and probe field amplitudes is enhanced. This is emphasized in Fig. 4, where cases of different values of the pump amplitude are considered. We clearly show an attenuation of the small peak for increasing values of the pump amplitude, which indicates that the time dependences of $I^{(4)}_{SFG}(\vec{k}_{SF},\Delta_{ir\text{-}IR},\Delta_{ir\text{-}vis})$ and $I^{(2\text{-}4)}_{SFG}(\vec{k}_{SF},\Delta_{ir\text{-}IR},\Delta_{ir\text{-}vis})$ becomes more similar due, in part, to the attenuation of the self-modulation term. Even if it is not possible to disentangle the field amplitude dependence of these contributions, because we are dealing here with intensities and not polarizations, at least we want to stress that the result is very sensitive to the relative values of the infrared pump and probe amplitudes. However, the amplitude of the visible field does not affect these time dependences, since it acts only once for each type of term. Next, in Fig. 5, we analyze the influence of the total decay rate Γ_{2222} on the time-resolved profile. Assuming the same resonant condi-

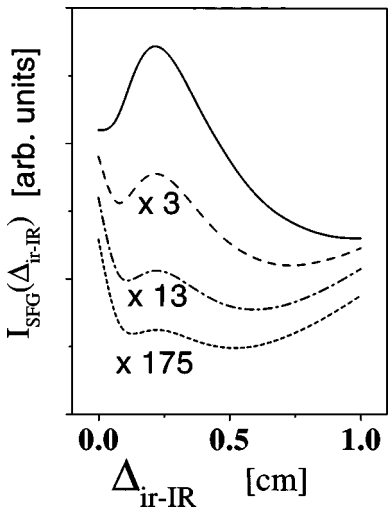

FIG. 4. We draw the same variations as in Fig. 3. Here the emphasis is on the influence of the field amplitudes on the central peak observed near the minimum of the time-resolved profile. The values are chosen as $\times 1$ for $E(\omega_{ir})=E(\omega_{vis})=E(\omega_{IR}),\times 3$ for $E(\omega_{ir})=E(\omega_{vis})=0.75\times E(\omega_{IR}),\times 13$ for $E(\omega_{ir})=E(\omega_{vis})=0.5\times E(\omega_{IR})$, and $\times 175$ for $E(\omega_{ir})=E(\omega_{vis})=0.25E(\omega_{IR})$. The vertical scale is enlarged according to the value indicated on each curve. The parameters are the same as in Fig. 3.

tions as in Fig. 5, we consider the cases of various Γ_{2222}. As expected, an increase of the total decay rate induces an overall decrease of the time-resolved profile. In addition, we note the disappearance of the central peak, an observation which is easily understandable. Here, with the increase of the total decay rate, the lifetime of the excited state $|2\rangle$ becomes shorter and shorter, and the time dependences of the terms $I^{(4)}_{SFG}(\vec{k}_{SF},\Delta_{ir\text{-}IR},\Delta_{ir\text{-}vis})$ and $I^{(2\text{-}4)}_{SFG}(\vec{k}_{SF},\Delta_{ir\text{-}IR},\Delta_{ir\text{-}vis})$ become comparable. As a consequence, we recover a similar time

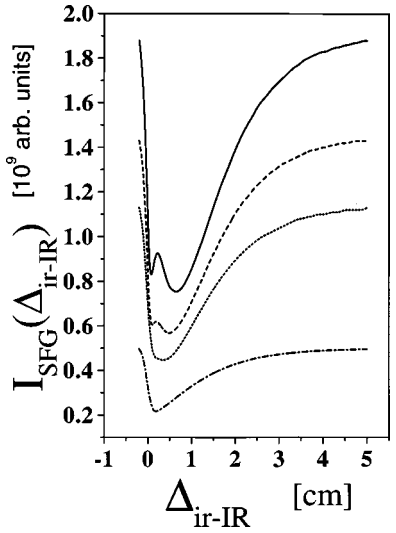

FIG. 5. We draw the time-resolved profiles associated with different values of the total decay rate Γ_{2222}. The continuous, dashed, short-dashed, and dot-dashed lines correspond to $\Gamma_{2222}=1$, 2.5, 4, and 10.0 cm^{-1}, respectively. All other parameters are identical to those used in Fig. 3.

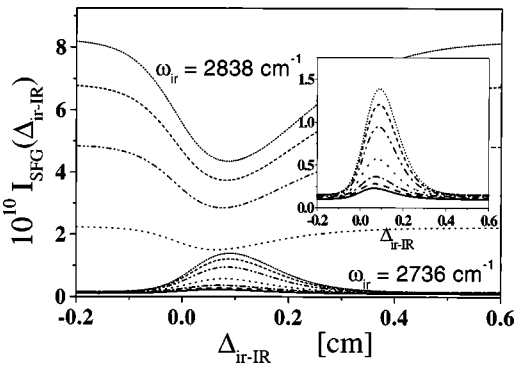

FIG. 6. Influence of the pure dephasing processes $\Gamma^{(d)}_{12}$ on the time-resolved profiles with an infrared probe field resonant with the first $\omega_{ir}=2838\ cm^{-1}$ or the second $\omega_{ir}=2736\ cm^{-1}$ vibrational transition. All the other parameters are identical to Fig. 3. In the inset, we emphasize the variations for the case $\omega_{ir}=2736\ cm^{-1}$. We just recover the variation arising from the depopulation of the second vibrational state. The values of the pure dephasing are $\Gamma^{(d)}_{12}=1.5\ cm^{-1}$ (short-dotted line), 3 cm^{-1} (short-dashed line), 6 cm^{-1} (dot-dot-dashed line), 15 cm^{-1} (dotted line), 30 cm^{-1} (dot-dashed line), 45 cm^{-1} (dashed line), and 60 cm^{-1} (plain line).

dependence in the individual contributions, and the central peak disappears. Next we study the influence of the pure vibrational dephasing for an infrared pump field resonant with the first vibrational transition, $\omega_{IR}=\omega_{21}$ and an infrared probe field resonant either with the first or second vibrational transition: $\omega_{ir}=2838$ or 2736 cm^{-1}. In Fig. 6, we show the influence of the pure vibrational dephasing constant $\Gamma^{(d)}_{12}$ of the first vibrational transition on the time-resolved profiles obtained for both infrared probe frequencies. No central peak is observed because of the particular values of the field amplitudes and vibrational dephasing constants considered here. In addition, $\Gamma^{(d)}_{12}$ pertains to the range where the pure dephasing predominantly drives the dynamical evolution. In addition, the influence of the dephasing processes is comparable for physical processes initiated either from the ground vibrational state or from the first excited vibrational state. The variations represented on the inset clearly show that the SFG intensity retains the same time dependence for different vibrational dephasing constants. Only an overall decrease of the time-resolved profile is observed. This variation straightforwardly follows the time dependence of the population created by the pump pulse in the first excited state. Finally, it has to be noted that both experimental situations $\omega_{ir}=\omega_{21}$ and $\omega_{ir}=\omega_{32}$ are influenced similarly by the pure dephasing constants. The same type of variations are considered in Fig. 7 to analyze the influence of the pure dephasing processes $\Gamma^{(d)}_{23}$ taking place on the second vibrational transition—that is to say, between levels $|2\rangle$ and $|3\rangle$. The situation is more complicated here. First of all, we see that pure dephasing processes are more efficient on a SFG signal created from the excited state than from the ground state. This can be understood easily. For the case where the infrared probe field is resonant with the first vibrational transition, $\Gamma^{(d)}_{23}$ does not participate in the dynamics underlying the polarization term $\vec{P}^{(2)}(\vec{k}_{SF},t)$ or in the main contributions of the polarization

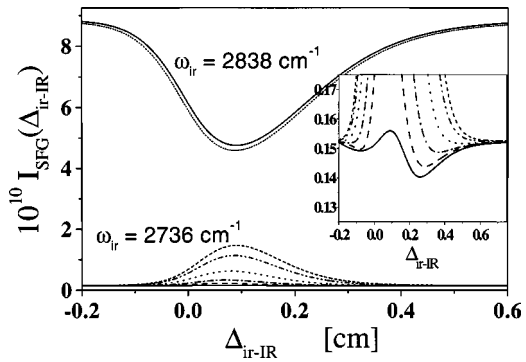

FIG. 7. Influence of the pure dephasing processes $\Gamma_{23}^{(d)}$ on the time-resolved profiles with an infrared probe field resonant with the first $\omega_{ir}=2838\,\mathrm{cm}^{-1}$ or the second $\omega_{ir}=2736\,\mathrm{cm}^{-1}$ vibrational transition. All the other parameters are identical to Fig. 3. In the inset, we emphasize the interferences due to the mixing of $\vec{P}^{(2)}$ and $\vec{P}^{(4)}$ for the case $\omega_{ir}=2736\,\mathrm{cm}^{-1}$. The values of the pure dephasing are $\Gamma_{12}^{(d)}=1.5\,\mathrm{cm}^{-1}$ (short-dotted line), 3 cm^{-1} (short-dashed line), 6 cm^{-1} (dot-dot-dashed line), 15 cm^{-1} (dotted line), 30 cm^{-1} (dot-dashed line), 45 cm^{-1} (dashed line), and 60 cm^{-1} (plain line).

term $\vec{P}^{(4)}(\vec{k}_{SF},t)$. Of course, some pathways participating in $\vec{P}^{(4)}(\vec{k}_{SF},t)$ go through state $|3\rangle$, and therefore give a dependence on $\Gamma_{23}^{(d)}$, but their contributions are small. However, for an infrared probe field resonant with the second vibrational transition, the dominant contributions involve pathways going through the transition $|2\rangle\leftrightarrow|3\rangle$. This is why the influence of $\Gamma_{23}^{(d)}$ is stronger for an infrared probe beam resonant with the second vibrational transition. Finally, in the inset, we note an unusual variation of the time-resolved profile showing a PSFG signal intensity which can be even smaller than the SFG signal intensity alone. These variations arise from interferences taking place between different pathway contributions to $\vec{P}^{(4)}(\vec{k}_{SF},t)$ whose contributions become competitive due to the fact that the resonant conditions for both experimental situations are better satisfied for increasing values of the pure dephasing constant $\Gamma_{12}^{(d)}$.

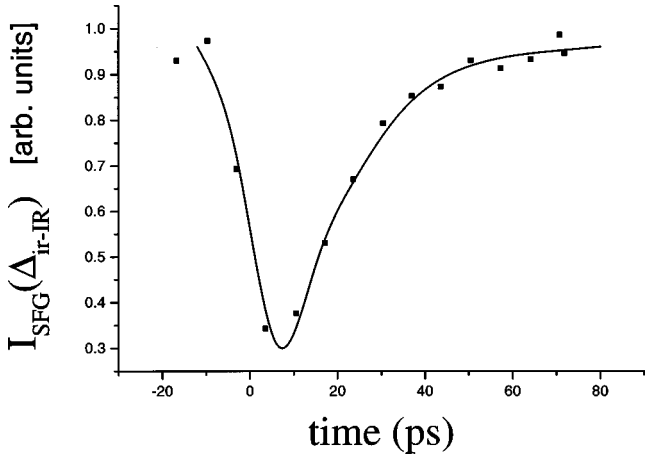

FIG. 8. We fit the experimental data (squares) obtained from Ref. [43] for an infrared probe beam resonant with the first vibrational transition, $\omega_{21}=\omega_{ir}=2838\,\mathrm{cm}^{-1}$. The values of the physical parameters are taken from the experiment.

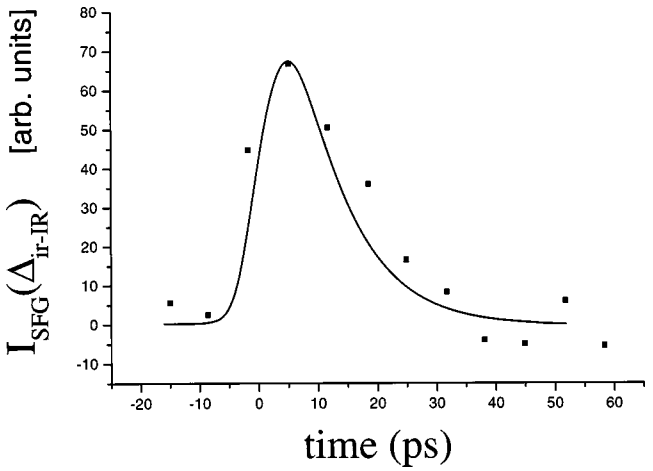

FIG. 9. We fit the experimental data (squares) obtained from the experiment of Chin *et al.* [43], and considered in Fig. 8. Here, the infrared probe beam is resonant with the second vibrational transition, $\omega_{32}=\omega_{ir}=2736\,\mathrm{cm}^{-1}$. The other parameters are identical to those in Fig. 8.

Finally, in the two last figures, 8 and 9, we fit the SFG signal intensity obtained for the C-H stretching modes on the hydrogen-terminated F/C(111)-(1×1), and corresponding to both resonant cases previously mentioned. We clearly show that a proper account of the dephasing constants gives a good fit of both experimental data. Note that all the parameters, except the infrared probe frequency, must simultaneously fit these data. As previously mentioned, the time dependence, and more precisely the position of the extremum, are very sensitive to the total decay rate Γ_{2222} and dephasing constant Γ_{1212} for $\omega_{ir}=\omega_{21}$, and with the additional dephasing constant Γ_{2323} for $\omega_{ir}=\omega_{32}$. For physical parameters which are very sensitive to the time dependence, we obtain $\Gamma_{2222}=2.5\,\mathrm{cm}^{-1}$, $\Gamma_{1212}^{(d)}=3.5\,\mathrm{cm}^{-1}$, and $\Gamma_{2323}^{(d)}=4.5\,\mathrm{cm}^{-1}$. Of course, the electronic dephasing is not accessible in this experiment due to the nonresonant conditions for the visible field. Again, the relative values of the field amplitudes have a strong influence on the time dependence of the signal intensity because they strongly modify the population and coherent contributions to the SFG signal intensities.

IV. CONCLUSION

In the present work, we have developed a unified description of pumped sum-frequency generation valid on the full scale of dephasing times for steady-state or pulsed experiments, which appears to be very powerful to study and test bonding processes on adsorption, as well as molecule-surface reactions [51,52]. The same methodology can be applied to a study of any type of wave mixing, provided that the spectral decomposition of the Liouvillian evolution operator can be obtained. This is due to the fact that the multiple time integral involving this type of pulse shape results in a recurrent form which can be extended to higher order. This approach opens new possibilities to study the influence of vibrational and electronic dephasings on the time depen-

dence of the transient sum-frequency signals, which were previously limited to very short dephasing times. We have shown, in the particular case of coincident infrared and visible probe pulses, that pure vibrational dephasings acting on successive vibrational transitions can be determined by using different resonant conditions for the infrared probe beam. Finally, with the possibility of exploring the complete range of dephasing times, we have been able to obtain a convenient fit of the experimental time-resolved profile obtained by Chin *et al.* on the C-H stretching mode. From this fit, the dephasing times of the first and second vibrational transitions of this mode were determined. More complex situations, involving for example time-delayed infrared and visible probe pulses [52,53], which are required for a study of the dynamical evolution in the highly excited vibrational states, can be handled with this description.

[1] X. D. Zhu, H. Suhr, and Y. R. Shen, Phys. Rev. B **35**, 3047 (1987).
[2] P. Guyot-Sionnest, J. Hunt, and Y. R. Shen, Phys. Rev. Lett. **59**, 1597 (1987).
[3] R. Superfine, J. Y. Huang, and Y. R. Shen, Phys. Rev. Lett. **66**, 1066 (1991).
[4] T. F. Heinz, F. J. Himpsel, E. Palange, and E. Burstein, Phys. Rev. Lett. **63**, 644 (1989).
[5] M. Y. Jiang, G. Pajer, and E. Burstein, Surf. Sci. **242**, 306 (1991).
[6] M. Y. Jiang, G. Pajer, E. Burstein, M. Yeganeh, and A. Yodh, Bull. Am. Phys. Soc. **37**, 652 (1992).
[7] B. N. J. Persson and R. Ryberg, Phys. Rev. Lett. **48**, 549 (1982).
[8] B. N. J. Persson, F. M. Hoffman, and R. Rydberg, Phys. Rev. B **34**, 2266 (1986).
[9] P. Guyot-Sionnest, P. Dumas, Y. J. Chabal, and G. Higashi, Phys. Rev. Lett. **64**, 2156 (1990).
[10] P. Guyot-Sionnest, Phys. Rev. Lett. **67**, 2323 (1991).
[11] J. C. Owrutsky, J. P. Culver, M. Li, Y. R. Kim, M. J. Sarisky, M. S. Yeganeh, A. G. Yodh, and R. M. Hochstrasser, J. Chem. Phys. **97**, 4421 (1992).
[12] J. H. Hunt, P. Guyot-Sionnest, and Y. R. Shen, Chem. Phys. Lett. **133**, 189 (1987).
[13] R. Superfine, P. Guyot-Sionnest, J. Hunt, C. Kao, and Y. R. Shen, Surf. Sci. **200**, 1445 (1988).
[14] J. Miragliotta, R. S. Polizotti, P. Rabinowitz, S. D. Cameron, and P. B. Hall, Appl. Phys. A: Solids Surfs **51**, 221 (1990).
[15] R. Raval, S. F. Parker, M. E. Pemble, P. Hollins, J. Pritchard, and M. A. Chesters, Surf. Sci. **203**, 353 (1988).
[16] R. P. Chin, J. Y. Huang, Y. R. Shen, T. J. Chuang, H. Seki, and M. Buck, Phys. Rev. B **45**, 1522 (1992).
[17] C. Stampfl, J. Neugebauer, and M. Scheffler, Surf. Sci. **307–309**, 8 (1994).
[18] H. Ishida and A. Liebsch, Phys. Rev. B **42**, 5505 (1990).
[19] F. Rebentrost and M. Kuchler, Appl. Phys. A: Mater. Sci. Process. **60**, 127 (1995).
[20] J. W. Gadzuk and A. C. Luntz, Surf. Sci. **144**, 429 (1984).
[21] B. N. Persson and M. Persson, Solid State Commun. **36**, 175 (1980).
[22] D. C. Langreth, Phys. Rev. Lett. **54**, 126 (1985).
[23] B. N. Persson, J. Phys. C **17**, 4741 (1984).
[24] J. C. Ariyasu, D. L. Mills, K. G. Lloyd, and J. C. Hemminger, Phys. Rev. B **30**, 507 (1984).
[25] M. Trenary, K. J. Uram, F. Bozso, and J. T. Yates, Surf. Sci. **146**, 269 (1984).
[26] J. C. Tully, Y. J. Chabal, K. Raghavachari, J. M. Browman, and R. R. Lucchese, Phys. Rev. B **31**, 1184 (1985).
[27] B. N. J. Persson and R. Ryberg, Phys. Rev. Lett. **54**, 2119 (1985).
[28] H. Morawitz, Phys. Rev. Lett. **58**, 2778 (1987).
[29] V. Pouthier, C. Ramseyer, and C. Girardet, J. Chem. Phys. **108**, 6502 (1998).
[30] V. Pouthier, Ph.D. thesis, Franche Comté University, Besançon, 1999.
[31] J. C. Ariyasu, D. L. Mills, K. G. Lloyd, and J. C. Hemminger, Phys. Rev. B **28**, 6123 (1983).
[32] Z. W. Gortel, H. J. Kreuzer, P. Piercy, and R. Teshima, Phys. Rev. B **36**, 3059 (1987).
[33] Y. J. Chabal, Surf. Sci. Rep. **8**, 211 (1988).
[34] W. Green-Johnson, J. Chem. Phys. **88**, 2939 (1988).
[35] M. Hutchinson and F. T. Georges, Chem. Phys. Lett. **124**, 211 (1986).
[36] R. M. Shelby, C. B. Harris, and P. A. Cornelius, J. Chem. Phys. **70**, 34 (1979).
[37] B. Fain and Z. W. Gortel, Physica B **159**, 361 (1989).
[38] Z. Ye, R. Tu, and P. Piercy, Phys. Rev. B **47**, 13 674 (1993).
[39] Z. Y. Zhang and D. C. Langreth, Phys. Rev. Lett. **59**, 2211 (1987).
[40] B. N. J. Persson and R. Ryberg, Phys. Rev. B **40**, 10 273 (1989).
[41] D. C. Langreth and M. Persson, Phys. Rev. B **43**, 1353 (1991).
[42] T. Yajima, H. Souma, and Y. Ishida, Phys. Rev. A **17**, 324 (1978).
[43] R. P. Chin, X. Blase, Y. R. Shen, and S. G. Louie, Europhys. Lett. **30**, 399 (1995).
[44] Y.-C. Sun, H. Gai, and G. A. Vith, J. Chem. Phys. **100**, 3247 (1994).
[45] A. L. Harris, L. Rothberg, L. H. Dubois, N. J. Levinos, and L. Dhar, Phys. Rev. Lett. **64**, 2086 (1990).
[46] A. L. Harris, L. Rothberg, L. Dhar, N. J. Levinos, and L. H. Dubois, J. Chem. Phys. **94**, 2438 (1991).
[47] A. L. Harris and L. Rothberg, J. Chem. Phys. **94**, 2449 (1991).
[48] T. Kato, M. Hayashi, A. A. Villaeys, and S. H. Lin, Phys. Rev. A **56**, 980 (1997).
[49] A. A. Villaeys and F. P. Lohner, Phys. Rev. A **59**, 3926 (1999).
[50] G. Placzek, in *Molecular Vibrations*, edited by E. Wilson, J. C. Decius, and P. C. Cross (Dover, New York, 1995).
[51] L. Chen, R. Wu, N. Kioussis, and Q. Zhang, Chem. Phys. Lett. **290**, 255 (1998).
[52] P. Guyot-Sionnest, P. Dumas, and Y. J. Chabal, J. Electron Spectrosc. Relat. Phenom. **54**, 54 (1998).
[53] A. A. Villaeys, V. Pflumio, and S. H. Lin, Phys. Rev. A **49**, 4996 (1994).